

Kinematics and Structure of the Starburst Galaxy NGC 7673

N. L. Homeier and J. S. Gallagher

Department of Astronomy, University of Wisconsin-Madison

ABSTRACT

The morphology and kinematics of the luminous blue starburst galaxy NGC 7673 are explored using the WIYN 3.5m telescope. Signs of a past kinematic disturbance are detected in the outer galaxy; the most notable feature is a luminous ripple located 1.55 arc minutes from the center of NGC 7673. Sub-arc second imaging in B and R filters also reveals red dust lanes and blue star clusters that delineate spiral arms in the bright inner disk and narrow band $H\alpha$ imaging shows that the luminous star clusters are associated with giant H II regions. The $H\alpha$ kinematics measured with echelle imaging spectroscopy using the WIYN DensePak fiber array imply that these H II regions are confined to a smoothly rotating disk. The velocity dispersion in ionized gas in the disk is $\sigma \sim 24 \text{ km s}^{-1}$, which sets an upper bound on the dispersion of young stellar populations.. Broad emission components with $\sigma \sim 63 \text{ km s}^{-1}$ found in some regions are likely produced by mechanical power supplied by massive, young stars; a violent starburst is occurring in a kinematically calm disk. Although the asymmetric outer features point to a merger or interaction as the starburst trigger, the inner disk structure constrains the strength of the event to the scale of a minor merger or weak interaction that occurred at least an outer disk dynamical time scale in the past.

Subject headings: Galaxies: Evolution, Galaxies: Kinematics and Dynamics, Galaxies: Starburst, Galaxies: Individual, ISM: H II regions

1. Introduction

High surface brightness blue galaxies have been a curiosity in samples of nearby galaxies for more than 40 years (e.g. Zwicky 1957, Sandage 1963). While these types of compact galaxies were often excluded from traditional samples of galaxies that chose objects on the basis of angular size (see Arp 1965), they can be readily found in surveys that select for blue colors or strong optical emission lines. Follow-up studies to the Markarian survey, for example, have shown that these high surface brightness galaxies consist of systems with AGNs and/or with extraordinarily high star formation rates (SFRs), i.e. the starburst galaxies (e.g., Sargent 1970, Huchra 1977). Recently interest in blue high SFR galaxies has been stimulated by their spectroscopic and morphological similarities to classes of galaxies which are commonly found at moderate to high redshifts (see Gallagher, Hunter, & Bushouse 1989, Gallagher 1990, Cowie, Hu, & Songalia 1995, Ellis 1997,

Guzman et al. 1998). Hence, studying nearby starbursts can further our understanding of rapidly evolving galaxies observed at moderate to large lookback times.

High surface brightness starburst galaxies with blue optical colors comprise about 5% of the local galaxy field population with optical luminosities of $L_B \gtrsim 3 \times 10^9 L_\odot$ (e.g. Huchra 1977). The origins, structures, and evolution of these luminous blue galaxies (LBGs), however, are not well-understood. We therefore have undertaken a new study of nearby LBGs with the objectives of obtaining better information on their structures, characterizing spatial patterns of star formation, and measuring internal kinematics. The dynamics of these systems are particularly important for predicting their subsequent evolution. Many of these galaxies are optically peculiar at the moment we see them, due to enhanced SFRs, but their appearance at later times may be determined by the present locations and kinematics of their stars and gas, which in turn influence future star formation processes.

In this paper we report results from a study of emission line kinematics and optical imaging with the WIYN¹ 3.5m telescope in the archetypal “clumpy irregular” galaxy NGC 7673² (Casini & Heidmann 1976, Tamura & Heidmann 1986, Benvenuti et al. 1982). This galaxy has a highly disturbed optical structure, which leads naturally to the question of its dynamical state. Is this a disrupted system, or an example of unusual star formation processes within a dynamically normal disk galaxy? A second paper in this series focuses on star formation patterns and timescales from high angular resolution imaging of NGC 7673 obtained with the Wide Field Planetary Camera 2 on the *Hubble Space Telescope* (Gallagher et al. 1999).

2. Properties of NGC 7673

The unusual optical structure of NGC 7673 (= IV Zw 149, Mrk 325) was initially described in terms of the presence of multiple bright knots (e.g., Markarian & Lipovetski 1971, Börngen & Kalloglian 1975). High quality ground-based images, primarily obtained by J. Heidmann and his collaborators, indicated this galaxy consists of giant star-forming clumps embedded in a diffuse halo, and thus NGC 7673 was classified as a clumpy irregular galaxy (Casini & Heidmann 1976, Coupinot et al. 1982). The superb ground-based images of Coupinot et al. (1982) also showed the spiral pattern that was noted in the RC2 and by Huchra (1977), which becomes clearer in images taken with WFPC2 (Gallagher et al. 1999). The hyperactive star formation within the clumps deduced by Heidmann and collaborators was confirmed by Gallego et al. (1996); their data indicate that $L(H\alpha)$ for the three largest is $2-8 \times 10^8 L_\odot$. These are each comparable to the

¹The WIYN Observatory is a joint facility of the University of Wisconsin-Madison, Indiana University, Yale University, and the National Optical Astronomy Observatories.

²The RC2 (de Vaucouleurs, de Vaucouleurs, & Corwin 1976) and Huchra (1977) classified NGC 7673 as a disturbed spiral, while Casini & Heidmann noted that large star forming clumps in an envelope are characteristic of luminous UV bright galaxies which they called ‘clumpy irregulars’, of which NGC 7673 is a prime example.

total $L(\text{H}\alpha)$ seen in many starburst galaxy nuclei.

Emission line kinematics were measured in NGC 7673 by Duflot-Augarde & Alloin (1982; hereafter DA), who found a remarkably constant velocity across the galaxy. The lack of internal velocity spread led DA to conclude that NGC 7673 is rather quiescent, and they therefore rejected a merger model, but noted that an interaction with its neighboring galaxy, NGC 7677 (Mrk 326) at a similar radial velocity (3554 km s^{-1} versus 3405 km s^{-1}), is possible, as suggested by Casini & Heidmann (1976). Further observations of the emission lines in NGC 7673 by Taniguchi & Tamura (1987) taken at higher spectral resolution showed the presence of a broad line component beneath the narrow emission line in clump B, the northwestern clump. They suggested that this broad feature, for which they measured a full width zero intensity (FWZI) of 420 km s^{-1} , is due to mass motions powered by supernova activity.

NGC 7673 appears to be a member of a small galaxy group that is relatively isolated, possibly located on the outskirts of the Pegasus I cluster and in front of the Pisces-Perseus chain. The immediate environment of the NGC 7673-7 pair was mapped in the HI 21 cm line by Nordgren *et al.* (1997), who find an H I mass of $3.6 \pm 0.5 \times 10^9 M_{\odot}$ for NGC 7673. Both galaxies contain extended HI disks; NGC 7673 is apparently nearly face-on with a modest HI-asymmetry to the west. NGC 7677 contains a small outer HI irregularity that points towards its neighbor, and is at nearly its radial velocity. Thus while an interaction is not excluded, there is no striking evidence for an on-going event in this system.

In this paper we assume $H_0 = 75 \text{ km s}^{-1} \text{ Mpc}^{-1}$. The recession velocity of 3405 km s^{-1} for NGC 7673 then implies a distance of 46 Mpc, and a linear distance of 222 pc per arcsec. Other parameters in the NASA/IPAC Extragalactic Database³ are $B_T^0 = 12.81$ implying $M_B = -20$ and blue global colors of $(B-V)_0 = 0.34$ and $(U-B)_0 = -0.38$.

Our observations and reductions are detailed in §2. In §3 we present our results, which are discussed in §4, while §5 contains a summary and conclusions.

3. Observations & Reductions

All observations were made with the WIYN 3.5m, f/6.5 telescope at the Kitt Peak National Observatory. All data reduction was performed with IRAF⁴.

³The NASA/IPAC Extragalactic Database (NED) is operated by the Jet Propulsion Laboratory, California Institute of Technology, under contract with the National Aeronautics and Space Administration.

⁴IRAF is provided by the courtesy of the National Optical Observatories, which are operated by the Association of Universities for Research in Astronomy, Inc., under cooperative agreement with the US National Science Foundation.

3.1. Optical Imaging

Images were obtained using a Tektronics 2048 x 2048 pixel CCD with a field of 6.7 x 6.7 arcmin and a scale of 0.195 arcsec per pixel. On November 13, 1996 a 500 s exposure was taken with a Harris R filter, and a 700 s exposure with a Harris B filter. The images were corrected for bias and zero level and flat-fielded with the ‘ccdproc’ task; cosmic rays were not removed. The seeing in these images is 0.”8.

Narrow band imaging was undertaken on July 24, 1997, a non-photometric night with moderately poor seeing. We were able to get 2 exposures taken with a redshifted H α filter, 1000 s and 631 s (cloud-dodging), and a 300 s exposure taken with a Harris R filter. The redshifted H α filter is centered at 6618 Å and has a width of 72 Å. Thus our H α narrow band images also include emission from [N II].

These H α and R images were processed in the same way as the earlier data, except that we removed cosmic rays from the pair of narrow band images. Both the combined H α and R image were scaled in such a way that subtracting the R image from the combined H α image canceled out field stars, producing a continuum-subtracted H α image. The seeing in this final H α image is about 1”.4.

3.2. DensePak Optical Spectroscopy

On October 23, 1997, two 1500s exposures were taken with the fiber array DensePak (see Barden et al. 1998) on the WIYN Nasmyth port. DensePak is a fixed array of 91 red-optimized fibers arranged in a 7 x 13 rectangle. Each fiber has a 3” diameter, and the fiber centers are each separated by 4” to form a 30” x 45” array. The fiber cable feeds the Bench Spectrograph, which for these observations was configured with a 316 line mm⁻¹ echelle grating and a grating angle of 62.581 degrees. We used the Bench Spectrograph camera and the 2048 x 2048 T2kC CCD detector with 24μm per pixel, for a wavelength coverage of approximately 6300 to 6730 Å with a reciprocal dispersion of 0.13 Å per CCD pixel.

A DensePak schematic is shown in Figure 1. There are 4 fibers placed off the corners of the array: numbers 8, 32, 68, and 90. We were able to use these for the intended purpose of sky subtraction because these fibers were not covering the H α emitting regions of the galaxy, so we did not have to move the telescope for a separate sky exposure. Also note the gaps in numbering; 23 and 28 have been skipped. Fibers 46 and 59 are dead.

Bias frames and dome flats were taken at the beginning and end of the night and combined during reduction with the IRAF task ‘dohydra’. For wavelength calibration, comparison spectra were taken with a ThAr lamp after each exposure. The 4 spectra from the sky fibers were combined to make a single sky spectrum and subtracted from each of the other fibers as part of the ‘dohydra’ procedure. Combining the 2 final zeroed, flat-fielded, sky-subtracted spectra was

accomplished with ‘scombine’ with reject=‘erreject’ to remove cosmic rays.

To estimate the error in our measurements, Gaussian profiles were fit to the night sky lines in the combined sky spectrum with the IRAF task ‘splot’. The observed wavelength of the $H\alpha$ line is close to 6638 Å over the entire galaxy, so comparison night sky lines were chosen near this wavelength. The FWHM resolution determined in this way is 32 km s⁻¹. The statistical uncertainty in central wavelength for a bright sky line refers to the scatter about the absolute wavelength, and is ≤ 0.05 Å, which corresponds to 2.3 km s⁻¹ at 6638 Å. However, in some cases the complex profiles or low signal-to-noise ratios of the $H\alpha$ emission lines makes the determination of accurate radial velocities difficult, yielding a greater uncertainty.

Gaussian emission profiles were assumed and fitting done with the IRAF task ‘splot’.

4. Results

4.1. Imaging

The deep R-band image is shown in Figure 2a.; an unsharp mask of the same image is shown in Figure 2b. Surrounding the bright central disk of NGC 7673 are several wispy, low-surface brightness features. In Figure 2b one can see a broad ‘bridge’ extending to the northwest connecting the inner disk to the first arc at 36” (8 kpc) from the galaxy center. The next arc, or ripple, can be seen in Figure 2a, located to the east at 52” (11.5 kpc) from the center. The most striking ripple is located to the west at 1’55 (21 kpc) from the center of the bright optical disk. This sharply defined arc was first reported by Dettmar et al. (1984), who suggested this feature either could be stars or an emission line region. In Figure 2b. there are several extensions to the main disk, most noticeably two on the eastern edge and one in the southwest corner. The linear feature north of NGC 7673 is a background galaxy, which is confirmed by its extreme redness in the B–R image and the Gallagher et al. (1999) WFPC2 images.

The R-band image is shown again in Figure 2c., with a stretch that shows the structure of the inner disk, including the central bar. That the light gray smudge in the SE corner is a background galaxy is confirmed from its B–R color and the WFPC2 images which reveal it to be a distant (and beautiful) spiral galaxy. A B–R color map is shown in Figure 2d. The B and R images have not been photometrically calibrated, so the color map is a B/R ratio map after standard reduction and sky subtraction. The spiral nature of the inner disk is clearly visible; there are prominent red dust lanes and bright blue clusters in this image. Unfortunately, we were not able to get color information on the outer ripples; they are too faint for reliable color measurements from these data. However, the ripples are present in both B and R images with comparable intensities, indicating that they are composed of stars.

A continuum subtracted $H\alpha$ image is shown in Figure 3. There are 3 main H II regions: the central ‘nucleus’, the large clump to the NE, and a smaller clump situated between the two. These

correspond to clumps A, B, and C, respectively, as referred to by DA and Taniguchi & Tamura (1987). In the SE corner there is a fainter $H\alpha$ ring, where it is possible to identify smaller H II regions. A bright cluster of stars seen in the B and R -band images is located on the northern side of this crooked 'arm', nestled between edges of ionized gas visible in the $H\alpha$ image. The gas directly between us and the cluster does not appear in the $H\alpha$ image, but the gas in the surrounding galaxy plane is brightly lit. The diffuse outer features are not detected in our narrow band $H\alpha$ image, consistent with our interpretation that they are starlight.

4.2. Spectroscopy

We performed a kinematic study of NGC 7673 using the DensePak fiber array and the $H\alpha$ emission line redshifted to near 6638 Å. To find fiber placement on the galaxy, the narrow band $H\alpha$ image, Figure 3, is compared to the DensePak map with flux in gray-scale, shown in Figure 4. The approximate placement of the DensePak array is marked with a box in Figure 3. Figure 4 was produced with the IRAF task 'sbands', taking the flux in a 10 Å wide band centered on 6638 Å and using 6 Å wide bands to the blue and red for continuum subtraction. The fiber diameter of 3" covers a linear distance of approximately 650 pc at NGC 7673, but we were not able to cover all of the main body of the galaxy with our single DensePak pointing.

4.2.1. Emission Profiles

No emission was detected in 29 of the 89 working fibers; the fiber illumination pattern is consistent with our $H\alpha$ image. Of the remaining 60 fibers, 32 had emission fit by a single Gaussian, and 28 were deconvolved into two Gaussian components, one broad and one narrow. It became clear that deconvolution was necessary when a single component fit left large, broad, asymmetric shoulders of emission; most of these broad lines are found in the northern half of the galaxy. Sample spectra are displayed in Figure 5.

Fibers on the southern part of the galaxy were fit by a single Gaussian, but in most cases small shoulders, or wings, of emission often remained. These wings are similar in shape to those in the middle of the array, but much less pronounced. Even in spectra with similar peak emission, the wings were smaller in the southern part of the galaxy. A deconvolution of these spectra into two components improved the fit, but with one or both of the components having a FWHM at or below the instrumental resolution. Therefore, these spectra were fit with a single Gaussian. Figure 6 is a plot of FWHM, corrected for the instrumental profile ($\text{FWHM}^2 = (\text{FWHM}_{\text{obs}})^2 - (32 \text{ km s}^{-1})^2$), versus position, which shows the distinct widths of the two components, and some scatter, but no systematic variation $> 10 \text{ km s}^{-1}$ in the FWHM of the narrow emission component over the galaxy.

Some spectra show what appear to be multiple peaks, perhaps due to emission from two or

more individual H II regions, or splitting from expanding shells or bubbles. Since most of these spectra have low S/N, a single-Gaussian fit was forced to recover a mean central velocity and a FWHM of dubious meaning. Such profiles were observed in 12 fibers; 6 had FWHMs consistent with the narrow component, and 6 had $\text{FWHM} > 90 \text{ km s}^{-1}$.

4.2.2. *Velocity Field*

The velocity field as measured by the heliocentric velocities of the narrow components is shown in Figure 7, where the velocity is in km s^{-1} and grayscale shading is used to help visualize the velocity field. Filled polygons indicate spectra with no narrow emission component. Fibers with broad emission but not narrow are thus represented by filled polygons; this includes fibers 55, 62, 72, 79, and 81. Fibers which were fit by both a narrow and a broad Gaussian are marked with a small cross above the velocity.

We find the narrow component velocity field to be fairly constant, with a radial velocity difference of only $\sim 60 \text{ km s}^{-1}$ across the galaxy regions covered by DensePak (the western side of the galaxy was not sampled). The maximum velocity is 3444 km s^{-1} in the SW corner, and falls to 3403 km s^{-1} at the northern edge. The minimum, 3392 km s^{-1} , occurs near the nuclear region, and the recession velocity of the nucleus itself is $\sim 3407 \text{ km s}^{-1}$. These results agree with previous measurements by DA. This also agrees with the H I data (Nordgren et al. 1997 which shows the peak emission to be at a heliocentric velocity of 3410 km s^{-1} . The precision of the DensePak absolute radial velocities is similar to that obtained from HI 21-cm line measurements.

The shallow velocity gradient across NGC 7673 indicates that the H II regions are confined to a dynamically cold rotating disk that is nearly face-on. The optical and H I morphology of NGC 7673 also suggest the presence of a disk, whose existence is confirmed by these emission line measurements showing rotation about its barred nuclear region. Although the disk shows signs of perturbation, such as copious star formation and a disturbed spiral pattern, it has survived the event which triggered the starburst and appears to be rotating smoothly.

The velocity gradient measured by optical emission lines (here, and by DA), although modest due to a small angle of inclination, differs from that of the H I disk (Nordgren et al. 1997). The western edge of the optical disk is approaching and the eastern receding, but the H I velocity gradient is in the opposite sense. This may be a signature that moderate-scale kinematic disturbances remain in the disk of NGC 7673, and high angular resolution H I maps would provide a useful diagnostic of the state of this galaxy.

5. Discussion

5.1. Kinematics

In regions of low flux, the emission line profiles are usually Gaussian in shape; however, as previously mentioned, 12 fibers contain spectra with large asymmetries. Over the central regions of the galaxy where the flux is highest, we find H α emission lines with a relatively narrow core and broad wings, very similar to the integrated profiles of giant H II regions found in many previous studies (Smith & Weedman 1970, Gallagher & Hunter 1983, Skillman & Balick 1984, Arsenault & Roy 1986, Roy, Arsenault, & Joncas 1986, Arsenault & Roy 1988, Rozas et al. 1998). Some of these emission lines are well fit by a Voigt profile, but most have asymmetric shoulders, and thus are best fit with two Gaussian components. We therefore assume that the emission line profiles which resemble Voigt profile are a combination of two Gaussian components with negligible velocity offset, and fit all such profiles with two Gaussians, leaving the central wavelengths and line widths free to vary. Taking the emission component(s) in each fiber, we find the mean FWHM of each kinematic component is 56 and 149 km s⁻¹, respectively ($\sigma \sim 24$ km s⁻¹, $\sigma \sim 63$ km s⁻¹). Fibers with emission lines which were fit with two profiles are marked with a small cross in Figure 7. Most of the broad components are at a slightly lower velocity relative to the narrow line in the same spectrum, but never by more than 10 km s⁻¹. Taniguchi & Tamura (1987) also found a narrow and a broad component in the H α emission line from clump B; they measured the broad component as having a FWHM > 200 km s⁻¹, and found it was redshifted by 13 km s⁻¹ relative to the narrow component of FWHM ~ 70 km s⁻¹.

The mean FWHM of the narrow component is much broader than emission from typical H II regions in our own galaxy (typical FWHM ~ 25 km s⁻¹, see Münch 1958, Fich, Treffers, & Dahl 1990). The origin of ionized gas with supersonic velocity dispersions is still a subject of debate, and thus a generally accepted model for this phenomenon does not yet exist. An L- σ (luminosity-velocity dispersion) and D- σ (size-velocity dispersion) correlation for giant H II regions has been firmly established (see Melnick 1977, Terlevich & Melnick 1981, Arsenault & Roy 1988), but it is still not clear what this relationship means. L and D should correlate with mass; therefore one expects the velocity dispersion to also increase. However, the energy input to the ISM in the form of ionizing photons, stellar winds, and supernovae should also correlate with L and D, increasing the amount of ionized structure (expanding shells, filaments, etc.) and turbulent motions, both of which may broaden the integrated emission profiles.

There is evidence that apertures which include multiple ionized structures at various velocities can create a smooth Gaussian profile with a broadened core (Chu & Kennicutt 1994, Yang et al. 1996). In a study of NGC 604, the brightest H II region in M33, Yang et al. (1996) showed that although some of the broadening in the integrated profile is due to averaging over many emitting regions, the mean corrected FWHM still shows a substantial velocity dispersion above that expected from purely thermal broadening. They concluded that the extra 30 km s⁻¹ could be explained as virial motions. This is in contrast to the case of the 30 Doradus giant H II region as examined by Chu & Kennicutt (1994), where even a tenfold increase in the estimated mass of the region yielded a gravitational velocity dispersion that was negligible in comparison with the

observed dispersion. In this case the conclusion was that the dominant contribution to the global velocity dispersion in 30 Dor is from shell motions, but with turbulence also playing a role.

It is not clear what is causing the width of the narrow emission cores in the case of NGC 7673. If it is due to gravitational motions, we should expect to see wider lines in connection with the more massive H II regions as shown in the H α image. Broadening due to averaging over many bubbles and filaments should also produce a spatial variation in the line widths, as some fibers cover a greater number of H II regions than others. Due to the low spatial resolution of our observations and the uncertainty in fiber placement, we cannot rule out either of these possibilities. The observed scatter of approximately 10 km s^{-1} in the total FWHM about the mean value implies an extra velocity component of width $\sim 35 \text{ km s}^{-1}$ (FWHM, or $\sigma \sim 15 \text{ km s}^{-1}$) is possible.

We also see a broad emission component underlying the (relatively) narrow cores, which have been previously observed in H α emission lines, but are not well-understood. Broadened cores produced by averaging over many emitting areas have been found accompanied by low-intensity wings (Chu & Kennicutt 1994), presumably from expanding shells and bubbles. The recent study of NGC 604 (Yang et al. 1996) also showed broad wings in the integrated profiles, again, from the inclusion of many expanding shells. It would be interesting to see if these integrated profiles can be deconvolved into narrow and broad components, and how the width and/or shape of the lines change as one averages over a larger area.

There are three leading explanations for the broad wings: they may be the result of integrating over many ionized structures at different velocities, or a broad emission component may be present from hot, turbulent gas confined to large cavities carved out by massive stars, or they could be due to some type of break-out phenomenon, such as a champagne flow or a starburst-powered galactic wind.

Massive outflow phenomenon is highly unlikely because of the absence of double-peaked emission profiles and/or a substantial velocity offset between the narrow and broad components, both of which are characteristic of superwinds (Heckman, Armus, & Miley 1990, Lehnert & Heckman 1996). This leaves us with the first two explanations as listed above. Given the results of the studies by Chu & Kennicutt (1994) and Yang et al. (1996), we favor the first explanation, where the line profiles are the result of integrating over many shells, bubbles, and filaments, which can also explain the highly supersonic line widths of the narrow component.

5.2. Starburst Trigger

NGC 7673 is a close projected companion to NGC 7677, which has a similar radial velocity; therefore these two galaxies are probably a physical pair (Casini & Heidmann 1976, Nordgren et al. 1997). The surrounding area is free of small H I sources. A few minor appendages to the main disk of NGC 7673 are seen in the low-resolution H I map of Nordgren et al. (1997), but there is an absence of classic interaction signatures, such as H I tails. Given the disturbed optical appearance

of NGC 7673, its overall H I morphology is surprisingly symmetric. No H I peculiarities near the location of the outer optical shell were detected, although this may be due to the low resolution of the H I map. As mentioned previously, there is a warp in the disk of NGC 7677 and an H I extension pointing towards NGC 7673, but the outer H I envelopes are widely separated. The H I structure in these galaxies displays no indications of a significant on-going interaction between the two; any serious interaction would need to have taken place long enough ago for the outer H I disks to recover to their observed relatively normal states.

The discrepancy between the morphology of NGC 7673 and NGC 7677 is apparent on the Digital Sky Survey⁵ frames; NGC 7677 looks relatively regular, with a bright nuclear region and grand design spiral arms, in dramatic contrast to NGC 7673, whose high levels of star formation create giant H II regions and a remarkably clumpy appearance. If the starburst in NGC 7673 is due to an interaction with NGC 7677, then the interaction scenario must be able to explain why NGC 7673 is so disturbed, and NGC 7677 relatively unscathed. We conclude that an on-going interaction with NGC 7677 is not the starburst trigger. Even though no strong collision is currently in progress between NGC 7673 and NGC 7677, the disturbed outer optical disk of NGC 7673 does seem to be the signature of a past interaction.

The sharp outermost arc, along with the wispy extensions and faint ripples that surround the bright inner optical disk, are features usually associated with merger candidate E, S0, and a few Sa galaxies (Schweizer & Seitzer 1988). These structures are rare in later-type galaxies, but have also been found around another spiral starburst galaxy, NGC 3310 (Mulder & van Driel 1996). There are striking similarities between NGC 7673 and NGC 3310. They are both starburst galaxies with inner spiral structure surrounded by faint arcs and ripples, and their H α emission lines are strong and asymmetric (Grothues & Schmidt-Kaler 1991). The general consensus is that NGC 3310 has gone through a minor merger with a dwarf companion, which accounts for the starburst, peculiar arc, and ripple features in its outer parts (Grothues & Schmidt-Kaler 1991, Mulder & van Driel 1996, Smith et al. 1996, Mulder et al. 1995, Kikumoto et al. 1993). The minor merger model therefore is also attractive for NGC 7673.

Theoretical work concerning ripples and ‘shells’ around galaxies has shown that they can be formed in a variety of circumstances around both elliptical and disk galaxies (Quinn 1984, Wallin & Struck-Marcell 1988, Hernquist & Quinn 1989, Hernquist & Spergel 1992, Howard et al. 1993). Observationally, it is often difficult to distinguish between the models, and thus the origin of ripples in any particular object is often a subject of debate. Thus while mergers are the preferred model for the production of ripples and related features, their origin in other types of interactions cannot be excluded.

⁵The Digitized Sky Survey was produced at the Space Telescope Science Institute under U.S. Government grant NAG W-2166. The images of these surveys are based on photographic data obtained using the Oschin Schmidt Telescope on Palomar Mountain and the UK Schmidt Telescope. The plates were processed into the present compressed digital form with the permission of these institutions.

We therefore have two possible models: the NGC 7673 starburst could have been triggered by a past interaction with NGC 7677 that occurred long enough ago that any tidal streamers are gone, or a small galaxy could have merged with NGC 7673 in the past and the nearby presence of NGC 7677 is simply fortuitous. In either case the collisional event must have occurred long enough ago to allow the outer disk to mostly recover, and have been mild enough to avoid serious disruption of the main disk. Any interloper must therefore have been much smaller than the accreting galaxy, probably $< 10\%$ of the mass of the disk (Hernquist & Mihos 1995), making NGC 7673 a minor merger candidate.

6. Summary and conclusions

We have obtained moderate resolution optical images and echelle spectroscopy of the luminous blue galaxy NGC 7673. Our B-R color map shows red dust lanes and blue star clusters in an irregular spiral pattern, and the $H\alpha$ image confirms that these bright clusters are also giant H II regions. The deep B and R -band images confirm the presence of the previously reported ripple $1'.55$ west of the galaxy center (Dettmar et al. 1984), as well as revealing several other faint extensions and ripples surrounding the bright optical disk. These features are composed of stars, probably in the outer disk of NGC 7673.

Our fiber array measurements of the $H\alpha$ kinematics demonstrate that the H II regions are embedded in a smoothly rotating disk that we are viewing near a rotational pole. Despite the presence of a large-scale starburst, the disk velocity field appears to be remarkably regular. In areas of low flux, the emission profiles are often highly asymmetric, and are not well described by a single Gaussian profile. We may be seeing line splitting from isolated ionized super-shells, or the lines may be a combination of two or more H II regions with different radial velocities. Double Gaussian fits were performed on emission lines from the central regions of the galaxy to investigate the nature of the broad wings of emission. We find that a two component model, one narrow and one broad, fit the observed spectra rather well. The narrow component of complex emission line profiles have the same width as the single component lines, $\text{FWHM} \sim 55 \text{ km s}^{-1}$, and the broad component has a $\text{FWHM} \sim 150 \text{ km s}^{-1}$. The broad lines often have a slight velocity offset ($< 10 \text{ km s}^{-1}$), blue-ward of the narrow lines.

We can exclude an active interaction with NGC 7677 as the starburst trigger, but we cannot rule out a past interaction. If NGC 7677 is the culprit, then the starburst phase must be sustained well after the main encounter. The other possibility is capture of a dwarf companion, as in the case of NGC 3310, the leading candidate for a major starburst induced by a minor merger. The morphological similarities between NGC 7673 and NGC 3310 and NGC 7673's symmetric outer H I disk (Nordgren et al. 1997) lend support to the minor merger hypothesis. High resolution H I observations may resolve this issue.

It is a pleasure to thank the many people who make the WIYN 3.5-m an outstanding research telescope, and especially Sam Barden and Dave Sawyer for bringing DensePak online. We would like to thank Chris Dolan and Chris Anderson for their help with DensePak data reduction. We would also like to thank an anonymous referee for comments which improved the paper and for pointing out the possibly rather isolated location of NGC 7673. This project is a component of WFPC2 Investigation Definition Team studies of luminous blue galaxies, and is supported in part by NASA contract NAS 7-1260 to the Jet Propulsion Laboratory.

REFERENCES

- Arp, H. 1966, ApJ Supp. Ser. 14, 1
- Arsenault, R., & Roy, J.-R. 1986, AJ, 92, 567
- Arsenault, R., & Roy, J.-R. 1988, A&A, 201, 199
- Barden, S., Sawyer, D., & Honeycutt, R. 1998, Proc. SPIE, 3355, p.892-899
- Benvenuti, P., Casini, C., Heidmann, J. 1982, MNRAS, 198, 825
- Börngen, F., Kalloglian, A. 1975, ApJ, 11, 24
- Casini, C., & Heidmann, J. 1976, A&A, 47, 371
- Chu, Y., & Kennicutt, R. 1994, ApJ, 425, 720
- Coupinot, G., Hecquet, J., & Heidmann, J. 1982, MNRAS, 199, 451
- Cowie, L., Hu, E., Songalia, A. 1995, AJ, 110, 157
- Dettmar, R., Heidmann, J., Klein, U., & Wielebinski, R. 1984, A&A, 130, 424
- DeVaucouleurs, G., DeVaucouleurs, A., Corwin, H. 1976, 2nd Ref. Cat. of Bright Galaxies, U of Texas Press, Austin, TX
- Duflot-Augarde & Alloin, D. 1982 A&A, 112, 257
- Fich, M., Treffers, R., Dahl, G. 1990, AJ, 99, 622
- Ellis, R. 1997, ARAA, 35, 389
- Gallagher, J. 1990, in Evolution of the Universe of Galaxies, ASP Conf Series 10, ed. R. G . Kron, p157
- Gallagher, J., Hunter, D. 1983, ApJ, 274, 141
- Gallagher, J., Hunter, D., Bushouse, H. 1989, AJ, 97, 700
- Gallagher, J. S. & Gibson, S. J. 1994, in Panchromatic View of Galaxies - Their Evolutionary Puzzle, eds. G. Herster, Ch. Theis, J. Gallagher (Gif-sur-Yvette:Editions Frontiers), p.207
- Gallagher, J., Homeier, N., Griffiths, R., & WFPC2 IDT 1999, in preparation
- Gallego, J., Zamorano, J., Rego, M., Alonso, O., Vitores, A. G. 1996, A&AS, 120, 323
- Grothues, H., Schmidt-Kaler, Th. 1991, A&A, 242, 357
- Guzman, R., Jangren, A., Koo, D., Bershadsky, M., Simard, L. 1998, ApJ, 495, L13

- Heckman, T., Armus, L., Miley, G. 1990, ApJS, 74, 833
- Hernquist, L., & Mihos, J. 1995, ApJ, 448, 41
- Hernquist, L., Quinn, P., 1989, ApJ, 342, 1
- Hernquist, L., & Spergel, D. 1992, ApJ Letters, 399, 117
- Howard, S., Keel, W.C., Byrd, G., & Burkey, J. 1993, ApJ, 417, 502
- Huchra, J. 1977, ApJS, 35, 171
- Hunter, D. A., van Woerden, H., & Gallagher, J. S. 1994, ApJS, 91, 79
- Lehnert, M., Heckman, T. 1996, ApJ 472, 546
- Kikumoto, T., Taniguchi, Y., Suzuki, M., & Tomisaka, K. 1993, AJ, 106, 2, 466
- Markarian, B., & Lipovetski, V. 1971, Astrofisika, 7, 511
- Melnick, J. 1977, ApJ, 213, 15
- Mendez, D., Esteban, C. 1997, ApJ, 488, 652
- Mihos, J., Hernquist, L. 1994, ApJ, 425, L13
- Münch, G. 1958, Rev. Mod. Phys., 30, 1035
- Mulder, P., van Driel, W. 1996, A&A, 309, 403
- Mulder, P., van Driel, W., Braine, J. 1995, A&A, 300, 687
- Nordgren, T., Chengalur, J., Salpeter, E., & Terzian, Y. 1997, AJ, 114, 77
- Quinn, P., 1984, ApJ, 279, 596
- Roy, J., Arsenault, R., Joncas, G. 1986, ApJ, 300, 624
- Rozas, M., Sabalisk, N., Beckman, J., Knapen, J. 1998, A&A, 338, 15
- Sandage, A. 1963, ApJ, 138, 863
- Sargent, W., 1970, ApJ, 160, 405
- Schweizer, F., Seitzer, P. 1988, AA, 328, 88
- Skillman, E., & Balick, B. 1984 ApJ, 280, 580
- Smith, M., & Weedman, D. 1970 ApJ, 161,33

- Smith, D., Neff, S., Bothun, G., Fanelli, M., Offenberg, J., Waller, W., Bohlin, R., O’Connell, R., Roberts, M., Smith, A., & Stecher, T. 1996, *ApJ*, 473, L21
- Tamura, S., Heidmann, J. 1986, *Publ. Astron. Soc. Japan*, 38, 619
- Taniguchi, Y., & Tamura, S., 1987, *A&A*, 181, 265
- Terlevich, R., & Melnick, J. 1981, *MNRAS*, 195, 839
- Walker, I., Mihos, J., & Hernquist, L. 1996, *ApJ*, 460, 121
- Wallin, J., Struck-Marcell, C. 1988, *AJ*, 96, 1850
- Yang, H., Chu, Y.-H., Skillman, E., Terlevich, R. 1996, *AJ*, 112, 146
- Zwicky, F. 1957, *Morphological Astronomy* (Berlin: Springer Verlag).

Fig. 1.— The DensePak fiber array: each fiber has a $3''$ diameter; fiber centers are separated by $4''$, fiber numbers are also shown.

Fig. 2.— WIYN CCD images, north is up and east is to the left, (a)-(c) are R band: (a.) diffuse extensions (b.) outer arcs or ‘ripples’ (c.) inner structure (d.) B/R color map: red (black) dust lanes and blue (white) star clusters; Note the background galaxies are in the upper right and confused in the condensation to the southeast.

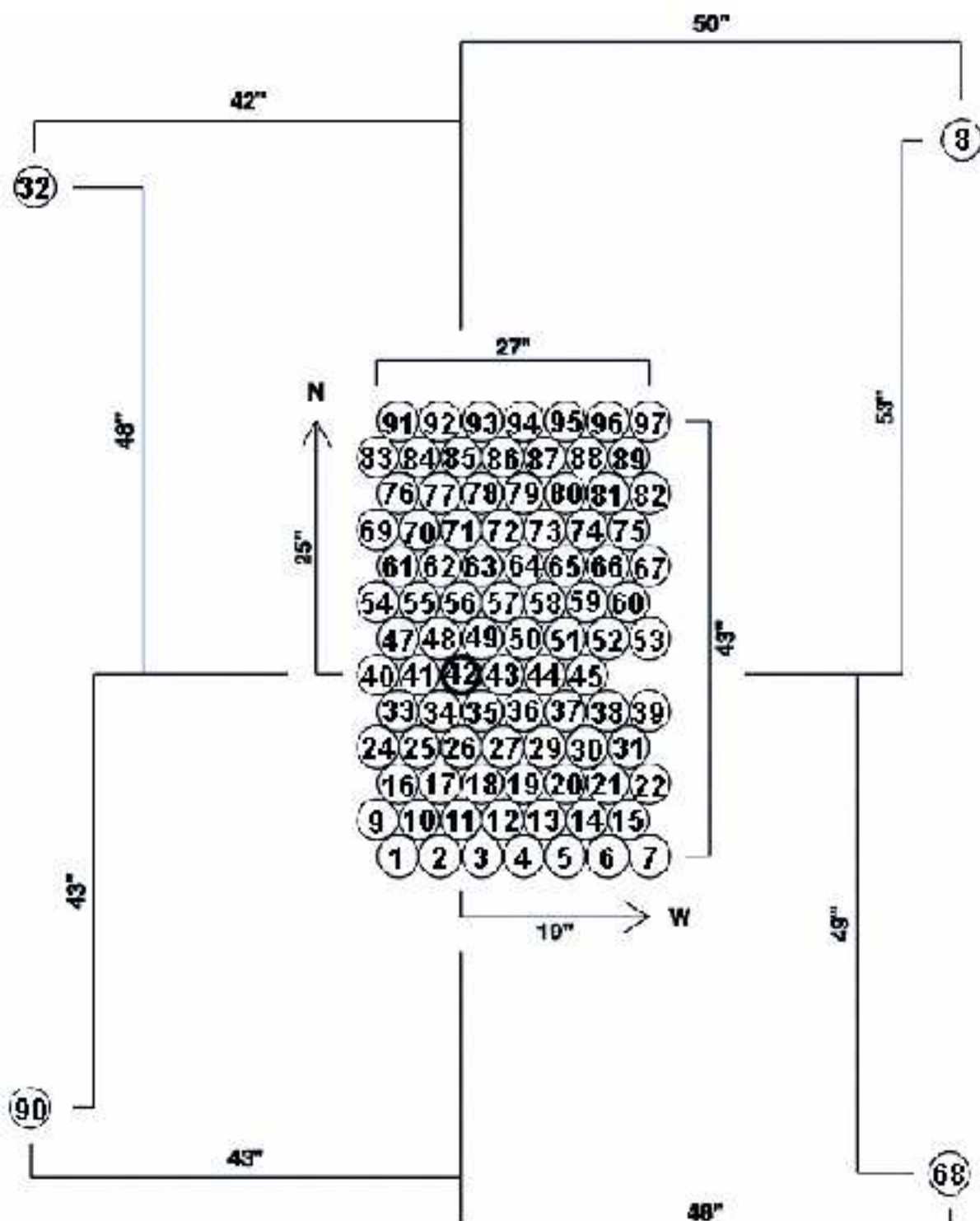
Fig. 3.— Continuum subtracted $H\alpha$ image, the box corresponds to placement of the DensePak array.

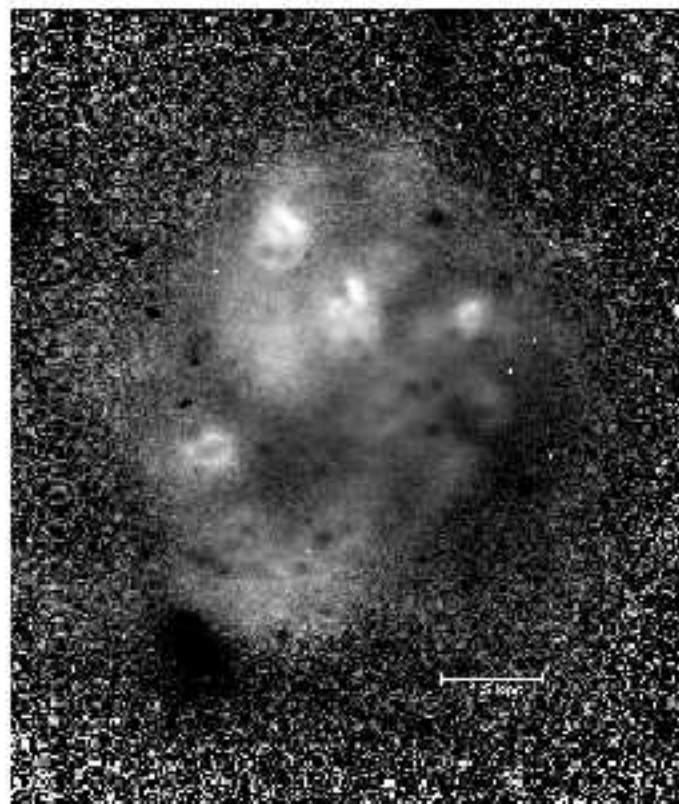
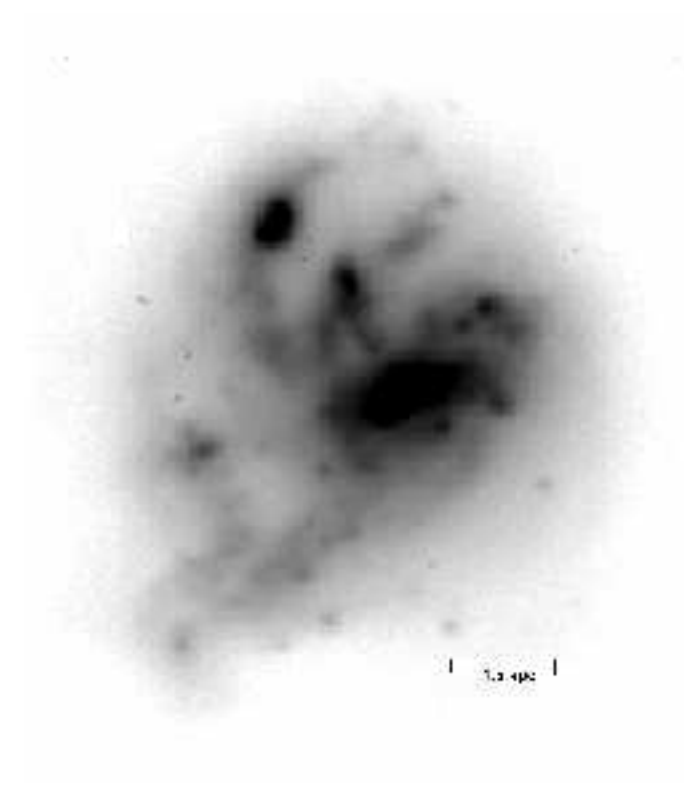
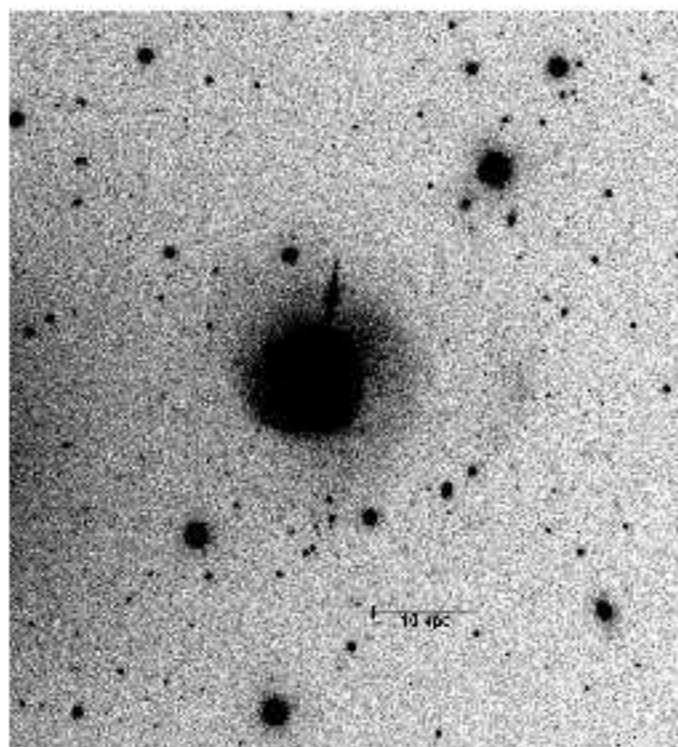
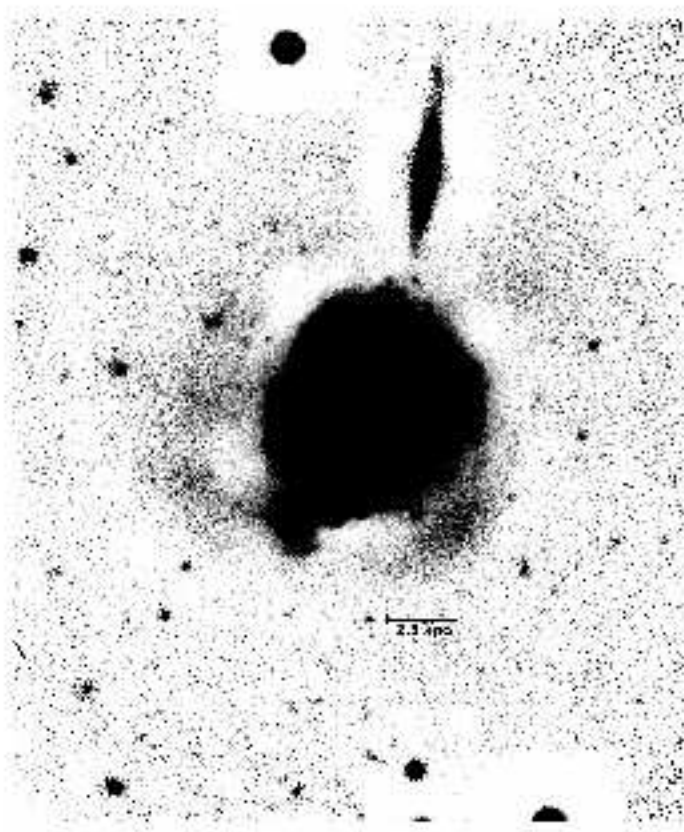
Fig. 4.— DensePak map, flux in grayscale. Fiber 39 is marked for orientation. North is up and east is to the left.

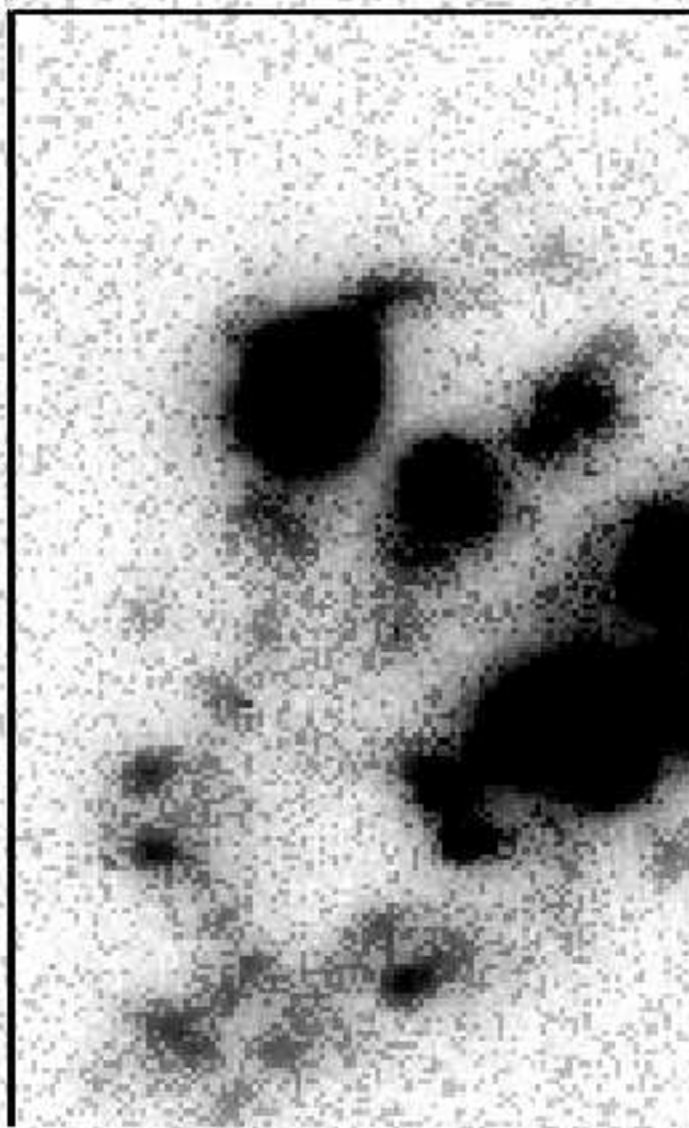
Fig. 5.— Examples of spectra with varying signal-to-noise, fiber number is at the top, solid line is the spectrum, dotted line is the fit. Note the broad wings in the fiber 57 spectrum.

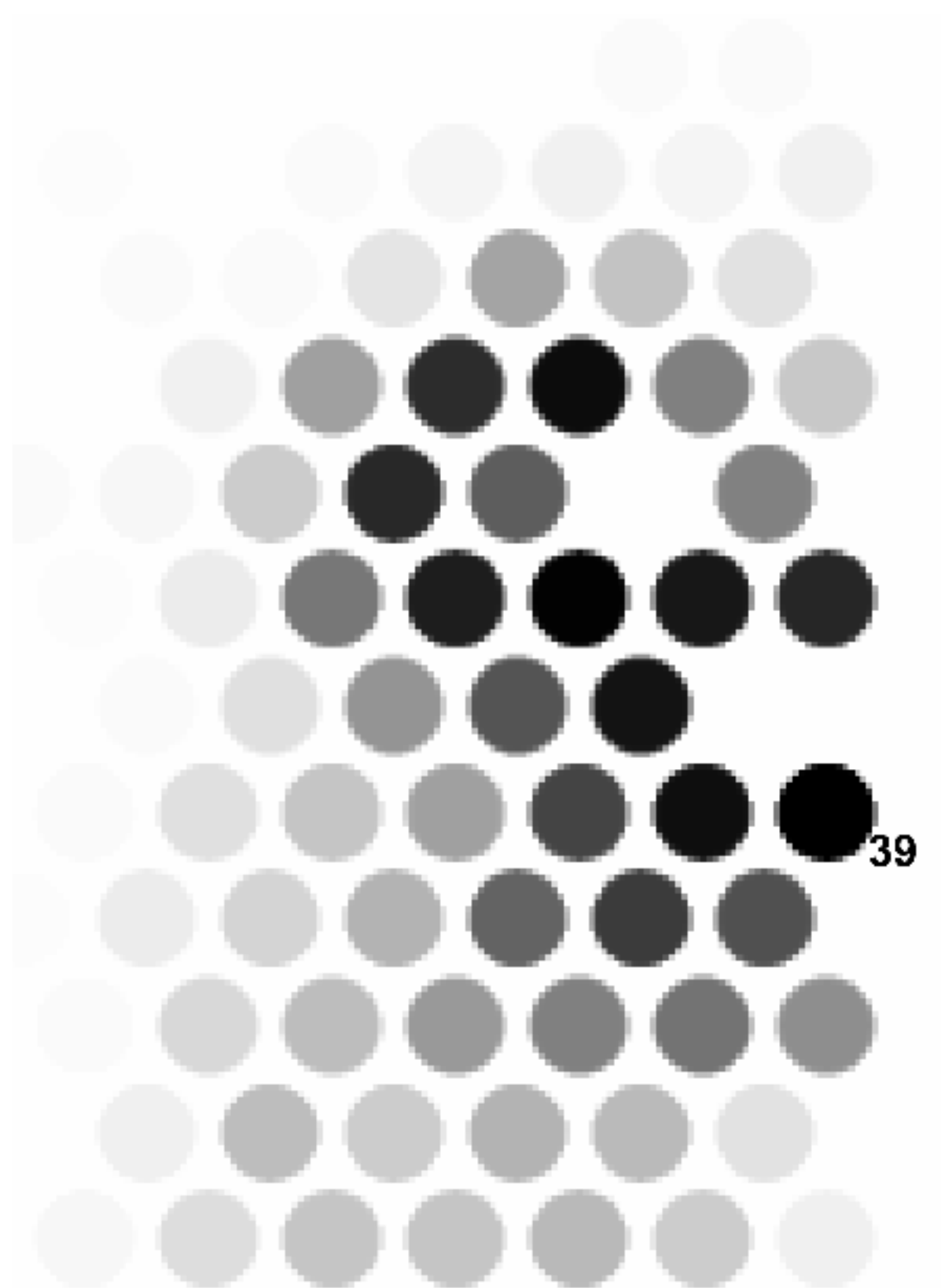
Fig. 6.— Position-FWHM diagram illustrating the lack of spatial variation in narrow line width. Plotted FWHMs are corrected for the 32 km s^{-1} instrumental broadening determined from night sky lines. Position is measured from the center of the southern-most row of fibers. The figure was made by plotting the FWHM values in each fiber along rows, all fibers in a row are at the same position value. The mean FWHMs of the two components are 56 and 149 km s^{-1} . Due to large asymmetries and/or low S/N, we have excluded fibers 16, 33, 41, 42, 48, 55, 62, 72, 75, 79, 80, and 81.

Fig. 7.— Heliocentric velocities of the narrow, $\text{FWHM} \sim 55 \text{ km s}^{-1}$, lines, in km s^{-1} . Fibers with no emission are colored black, and grayscale shading is included to aid visualizing the velocity field.









39

